

Laser Weldability of High-Strength Al-Zn Alloys and Its Improvement by the Use of an Appropriate Filler Material



JOSEPHIN ENZ, STEFAN RIEKEHR, VOLKER VENTZKE, NORBERT HUBER,
and NIKOLAI KASHAEV

Heat-treatable Al-Zn alloys are promising candidates for use as structural lightweight materials in automotive and aircraft applications. This is mainly due to their high strength-to-density ratio in comparison to conventionally employed Al alloys. Laser beam welding is an efficient method for producing joints with high weld quality and has been established in the industry for many years. However, it is well known that aluminum alloys with a high Zn content or, more precisely, with a high (Zn + Mg + Cu) content are difficult to fusion weld due to the formation of porosity and hot cracks. The present study concerns the laser weldability of these hard-to-weld Al-Zn alloys. In order to improve weldability, it was first necessary to understand the reasons for weldability problems and to identify crucial influencing factors. Based on this knowledge, it was finally possible to develop an appropriate approach. For this purpose, vanadium was selected as additional filler material. Vanadium exhibits favorable thermophysical properties and, thereby, can improve the weldability of Al-Zn alloys. The effectiveness of the approach was verified by its application to several Al-Zn alloys with differing amounts of (Zn + Mg + Cu).

DOI: 10.1007/s11661-016-3446-2

© The Minerals, Metals & Materials Society and ASM International 2016

I. INTRODUCTION

IN recent years, the economic and political pressure on the automotive and aircraft industry to reduce fuel consumption and CO₂ emissions has constantly increased. Because of this, the efforts for lightweight design became more important. A possibility for reducing weight of a structure is the use of lightweight and high-strength materials. Aluminum alloys are increasingly employed for diverse applications and also as a substitute for steel in many sheet applications. This is mainly due to their high strength-to-density ratio and machinability as well as their easy availability. Although heat-treatable Al-Zn alloys are attributed to the aluminum alloys with the highest strength, there is no widespread use of these alloys.^[1] The reason for this disregard of the industry lies in the fact that Al-Zn alloys exhibit distinct weldability problems such as the formation of porosity and hot cracking,

which predominantly arise during fusion welding.^[2–9] This is also the reason why only a few studies have been conducted on fusion welding these alloys. Up to now, defect-free welds were only achieved by solid-state welding processes such as friction stir welding.^[5,9] However, among the fusion welding processes, laser beam welding (LBW) belongs to the most efficient welding processes, due to high welding speeds, the high energy density of the laser beam, and the beneficial depth-to-width ratio of the resulting weld seams. Moreover, LBW possesses a higher flexibility—concerning the geometry and dimensions of the structure to be welded—in comparison to solid-state welding processes, due to the possibility of contactless welding and small beam dimension. By overcoming the weldability problems during LBW of Al-Zn alloys, these alloys may gain recognition as promising structural materials for lightweight structures. Recent work by Zhang *et al.* offers the first promising results in partially improving the weld quality by using a fiber laser for welding.^[10] However, further progress in this direction requires obtaining a deeper understanding of the existing weldability problems and, based on this, the development of welding processes that significantly reduce or avoid these problems.

The present study concerns the theoretical considerations of laser weldability of Al-Zn alloys. Significant factors were identified and their influence on weldability explained. Based on this knowledge, it was possible to develop an approach for improving the laser weldability of these hard-to-weld alloys, which includes the use of an additional filler material. The effectiveness of the

JOSEPHIN ENZ, PhD Student in the Department of Joining and Assessment, is with Helmholtz-Zentrum Geesthacht, Institute of Materials Research, Materials Mechanics, Max-Planck-Straße 1, 21052 Geesthacht, Germany, and also Scientist with TuTech Innovation GmbH, Harburger Schloßstraße 6-12, 21079 Hamburg, Germany. Contact email: josephin.enz@hzg.de STEFAN RIEKEHR and VOLKER VENTZKE, Scientists in the Department of Joining and Assessment, NORBERT HUBER, Head of the Division of Materials Mechanics, and NIKOLAI KASHAEV, Head of the Department of Joining and Assessment, are with Helmholtz-Zentrum Geesthacht, Institute of Materials Research, Materials Mechanics.

Manuscript submitted June 16, 2015.

Article published online April 1, 2016

approach was validated on several Al-Zn alloys with different Zn content.

II. LASER WELDABILITY OF AL-ZN ALLOYS

Weldability is generally defined as the ability of a material to be joined by a certain welding process such as LBW. It is primarily influenced by the chemical composition and metallurgical and thermophysical properties of the material, whereas welding parameters should play as much of a subordinate role as possible.^[11] In general, it can be stated that a material shows good weldability if the following is true: The less weld defects (such as pores and cracks) occur, the better the homogeneity of the weld microstructure or the less the resulting mechanical properties of the welded structure differ from the base material (BM). However, even in the case of weldable Al alloys with defect-free welds, a certain mechanical degradation is expected due to unavoidable microstructural changes during LBW.^[12]

It was shown in the work of Mondolfo and Ma that the total amount of Zn, Mg, and Cu of an Al-Zn alloy is a feasible indicator of that alloy's weldability.^[3,13] Al-Zn alloys with a high total amount of Zn, Mg, and Cu (above 9 wt pct) exhibit inferior weldability. Furthermore, it was indicated that a high Zn-to-Mg ratio has a similar effect on the weldability.^[3,13] By this means, it turns out that the weldability is particularly deteriorated by high Zn contents.

Rapp *et al.* and Leong *et al.* disclosed the physical fundamentals for understanding LBW of metals.^[14–16] It became apparent that the laser weldability of a metal strongly depends on its thermophysical properties. The relevant thermophysical properties of a selection of metals or alloying elements are shown in Table I.

For LBW—and, in particular, for deep penetration welding—melting and vaporization of the metal are required to form and to keep the keyhole open during welding. Therefore, the melting and vaporization temperature as well as the vapor pressure p_v of the alloying elements are crucial thermophysical parameters. From Table I and Figure 1(a), it becomes apparent that the melting and vaporization temperatures of Zn and Mg—the main alloying elements of Al-Zn alloys—are lower than those for Al. Furthermore, the vapor pressure of both elements is significantly higher than that for Al. This means that they easily vaporize during welding, which, on the one hand, helps keep the keyhole open in order to achieve a deep penetration of the keyhole^[14] but, on the other hand, leads to a loss of these volatile elements during welding.^[17] As a result, fine particles originating from the vaporization condensate on the workpiece surface in the form of a deposit. Another disadvantage is the irregular vaporization due to the depletion of Zn and Mg on the keyhole surface, which leads to a temporary vapor pressure drop and, hence, to a collapse of the keyhole.^[18] As a consequence of this, weld metal expulsion and porosity will occur—a type of porosity called keyhole-induced porosity.^[6] The dependence of the vaporization temperature on the alloying element content is shown in Figure 1(b). With an increasing amount of Zn and Mg, the vaporization temperature of the binary Al alloy is considerably reduced, whereas other alloying elements have almost no effect.^[14]

The counteracting pressure, which tries to close the keyhole during LBW, is the so-called keyhole pressure p_k . It includes capillary pressure p_c , dynamic pressure p_d , hydrostatic pressure p_h , and atmospheric pressure p_a , as described in detail in the work of Beyer.^[20] The capillary pressure has the largest effect on the keyhole pressure. It

Table I. Thermophysical Properties of Different Metals or Alloying Elements (According to Leong and Geyer^[15])

Thermophysical Parameter	Al	Zn	Mg	Cu	V
Melting point T_m [K (°C)]	933 (660)	693 (420)	923 (650)	1357 (1084)	2170 (1897)
Vaporization point T_v [K (°C)]	2743 (2470)	1180 (907)	1383 (1110)	2868 (2595)	3680 (3407)
Density ρ [10^3 kg m ⁻³] of					
Solid at 293 K (20 °C)	2.70	7.14	1.74	8.92	5.96
Liquid at T_m	2.38	6.58	1.59	8.00	5.36
Vapor pressure p_v (Pa) at					
T_m	10^{-6}	23	360	4.3×10^{-2}	3.3×10^{-3}
000 K (727 °C)	12×10^{-6}	12×10^3	1360	1.5×10^{-6}	0
2000 K (1727 °C)	900	n/a	n/a	380	3.1×10^{-4}
3000 K (2727 °C)	n/a	n/a	n/a	n/a	6.5
Viscosity μ (mPa s) at T_m	2	3.5	1.25	4.34	n/a
Surface tension γ (N m ⁻¹) at T_m	0.91	0.78	0.56	1.30	1.95
Thermal conductivity k [W m ⁻¹ (K) ⁻¹] of solid at T_m	210	9	130	330	50
Thermal diffusivity α (cm ² s ⁻¹) of solid at T_m	0.68	0.32	0.65	0.79	0.11
Specific heat capacity c_p [J/kg K] of solid at 293 K (20 °C)	897	388	1023	385	489
Absorptivity A [pct] at T_m or 300 K (27 °C) (*) for					
1.06 μ m (Nd:YAG)	11	42*	n/a	1.3*	45
10.6 μ m (CO ₂)	3	10	3*	5	5
Threshold irradiance I_m (MW cm ⁻²) for					
Nd:YAG	0.42	0.0032	n/a	n/a	0.099
CO ₂ with $d = 600$ μ m and $v = 4800$ mm/min	1.5	0.016	0.95	2.4	0.89

is defined by the surface tension of the liquid metal and the keyhole radius, which is assumed to be equal to the beam radius. In Figure 2, it can be seen that the capillary pressure decreases with the increasing beam diameter and reaches the lowest values for Mg and Zn because of the low surface tension. In order to achieve a stable keyhole, it is necessary for vapor and keyhole

pressure to compensate each other so that $p_v \geq p_k = p_c + p_d + p_h + p_a$.

The surface tension and viscosity of a liquid metal influence the melt pool behavior during welding. A low surface tension caused by Zn and Mg and a low viscosity caused by Mg typically lead to sagging of the melt pool and, hence, to closure and collapsing of the keyhole or to formation of spatter and spikes at the root side of the weld. The Cu—contained in Al-Zn alloys in lower

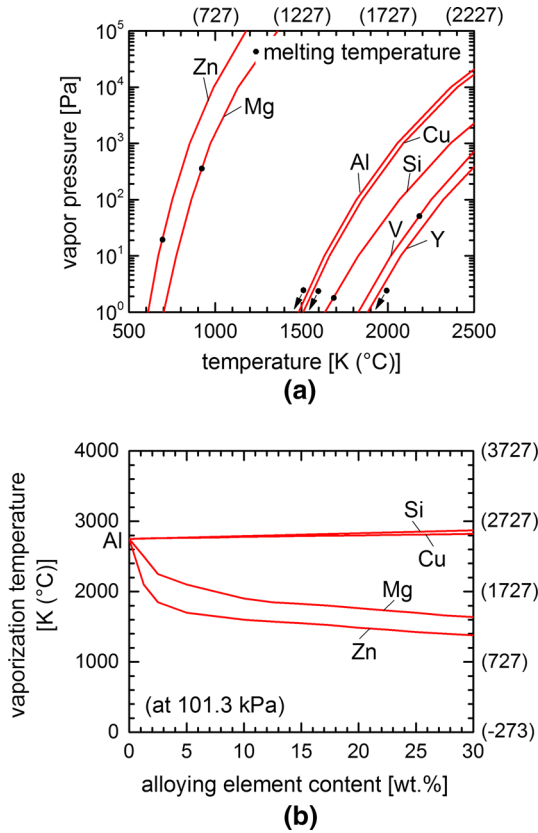


Fig. 1—(a) Vapor pressure of different metals as a function of temperature (according to Haynes^[19]) and (b) vaporization temperature of binary Al alloys as a function of the alloying element content (according to Rapp *et al.*^[14]).

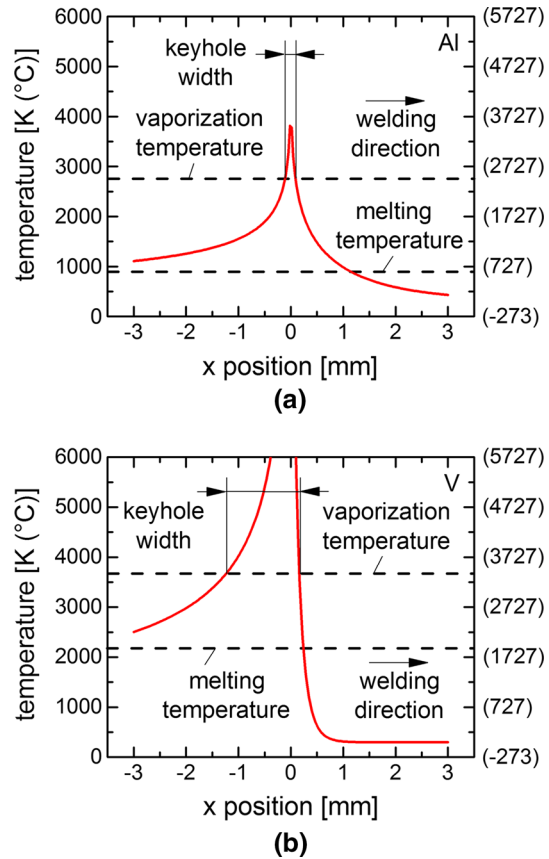


Fig. 3—Calculated temperature distribution during LBW of (a) an Al sheet and (b) a V sheet (calculated according to Table I).

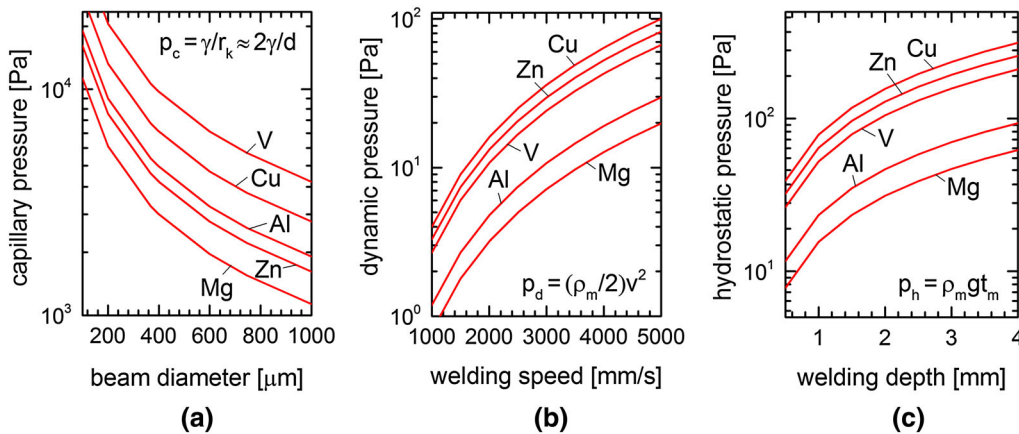


Fig. 2—Calculated capillary pressure (a), dynamic pressure (b), and hydrostatic pressure (c) of different metals (calculated according to Table I).

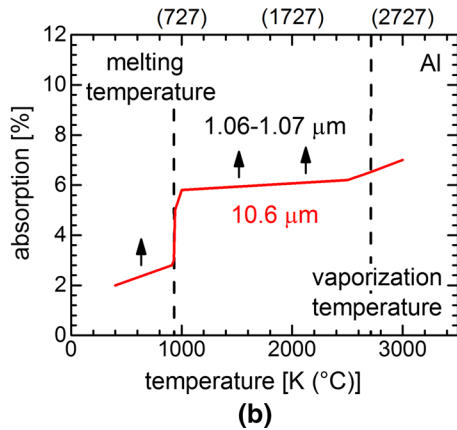
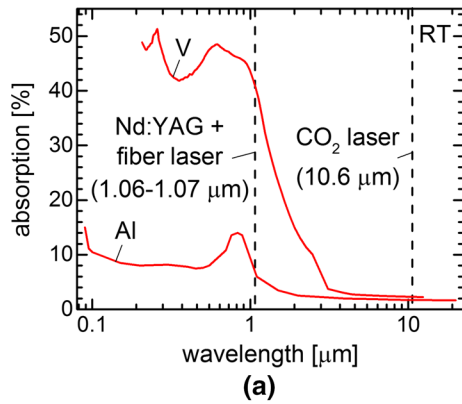


Fig. 4—Absorptivity of Al and V as a function of (a) wavelength and (b) temperature (according to Beyer^[20] and Guizzetti *et al.*^[22]).

concentrations as Zn and Mg—has a contrary effect (also Table I).

Regarding the temperature distribution during LBW, it can be seen that the thermal conductivity and diffusivity of a metal also influence the welding behavior. The temperature distribution during LBW can be easily calculated by the use of the model of a moving line source, which is described in detail, for example, by Beyer^[20] and Steen *et al.*^[21] The temperature T at position (x,y) in relation to the ambient temperature T_0 is given by $T(x,y) - T_0 = P/(t_s \rho c_p 2\pi\alpha) \cdot K_0(vr/2\alpha) \cdot \exp(vx/2\alpha)$, where P and v are the laser power and welding speed used for welding of a sheet with a thickness t_s . For the calculation, the modified Bessel function K_0 of the second kind and zero order is employed. By comparing the results for Al with vanadium (V) in Figure 3, it became obvious that Al exhibits a narrower keyhole—assuming that the keyhole is present—when the vaporization temperature is reached. This can be explained by the high thermal diffusivity and conductivity of Al, although the vaporization temperature is significantly lower.

The interaction between the laser beam and material is mainly defined by the absorptivity of a metal. In Figure 4, it can be seen that the absorptivity of a metal strongly depends on the wavelength of the laser used and the temperature of the metal. It can also be seen that the absorptivity of the Nd:YAG and fiber laser

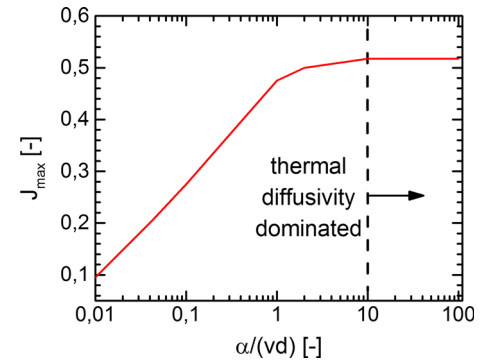


Fig. 5—Degree of interaction of laser beam and material (according to Leong *et al.*^[16]).

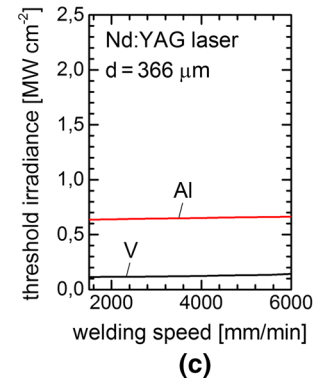
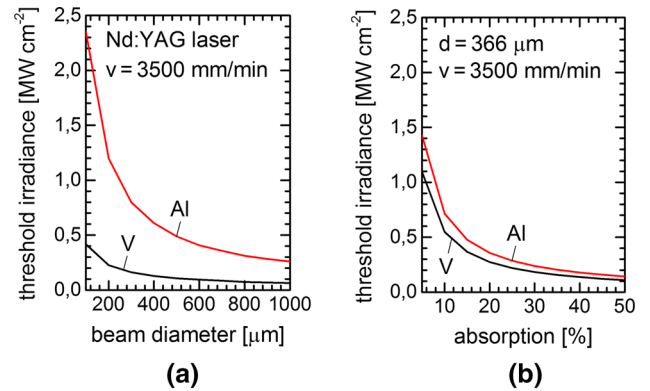


Fig. 6—Calculated laser beam irradiance as a function of (a) beam diameter, (b) absorption, and (c) welding speed (calculated according to Table I).

wavelength is more suitable for welding than the wavelength of a CO₂ laser. Further, with increasing temperature, the absorptivity is slightly increased. Of course, there are also other factors influencing the absorptivity, which are here neglected, due to their independence on the LBW process conditions.

Finally, the laser weldability of a metal can also be expressed in terms of laser beam irradiance. Leong and Geyer described the beam irradiance as a combination of the most important thermophysical properties of a metal in dependence of the used laser source.^[15] The threshold irradiance is given by $I_m = k(T_m - T_0)/(AdJ_{max})$, where k is the thermal conductivity of a metal,

T_m and T_0 are the melting and ambient temperatures, A the absorptivity of the surface for the laser beam, and d is the beam diameter at the surface. The degree of interaction of laser beam and material $J_{\max} = f(\alpha/vd)$ is a function of the thermal diffusivity α , the welding speed v , and the beam diameter d .^[16] Its value ranges from 0.1 to 0.51, as depicted in Figure 5. The threshold irradiance defines the minimum beam irradiance, which is required for welding. In Figure 6, the influence of metal, beam diameter, absorption, and welding speed is exemplarily shown. It can be easily seen that the threshold irradiance is highest for Al welded with a laser providing a small laser beam diameter, a low absorption (as in the case of a large wavelength), and high welding speeds. In this regard, the change of welding speed has the lowest influence on the threshold irradiance. The presence of weld pool instabilities can be expected, when high beam irradiances are applied to metals with low viscosity and low surface tension. Hence, only a narrow range of beam irradiance and process parameters may produce reasonable welds.

It has to be noted that another reason for porosity in Al welds is the presence of hydrogen in the melt pool. This can be explained by the high solubility of hydrogen in liquid Al, as shown in Figure 7(a). The hydrogen generally originates from the base and filler material in the form of an oxide layer and surface contaminations as well as

dissolved hydrogen in the bulk material. In this connection, the chemical composition and, in particular, the Mg content of the alloy have a significant influence on the hydrogen solubility (Figure 7(b)). Additionally, hydrogen can also originate from ambient air. In general, hydrogen-induced porosity appears to be considerably smaller in diameter in comparison to keyhole-induced porosity.^[6] However, by removing the oxide layer and by cleaning the surface prior to welding as well as by the use of shielding gas during welding, the hydrogen-induced porosity can be reduced to a minimum. However, even small hydrogen contents can cause porosity, as described by Mazur.^[24]

III. APPROACH FOR SOLVING THE WELDABILITY PROBLEMS OF AL-ZN ALLOYS

Based on the gained knowledge about the thermo-physical properties of metals and their influence on weldability, it was possible to identify an approach for solving the weldability problems of Al-Zn alloys.^[25,26]

This approach considers the use of an appropriate filler material, in addition to a conventional filler material, welded with a commonly used Nd:YAG laser. It can be seen from Table I that V is an appropriate candidate for an additional filler material. The reason for this is, on the one hand, the high absorptivity and the low beam irradiance of V, which denote good weldability, and, on the other hand, its high melting point and low vapor pressure, which inhibit an early vaporization and, thus, the formation of weldability problems. Other potential candidates with some promising thermophysical properties failed, due to one detrimental property. One such material is yttrium (Y). This material offers a high melting temperature and low vapor pressure, but due to its low surface tension, it does not improve the weldability. This was also proven in a preliminary study, where increased porosity occurred in a weld seam welded with Y foil as filler material.

The approach using V as additional filler material is validated in the following by its application to diverse Al-Zn alloys with differing amounts of (Zn + Mg + Cu), since a high Zn content in Al alloys is supposed to aggravate the weldability problems in terms of increased weld metal expulsion and porosity formation. In this context, especially, the effectiveness of the approach is most interesting for the high-alloyed Al-Zn alloys—with a high (Zn + Mg + Cu) content compared to standard Al-Zn alloys.

IV. MATERIALS AND EXPERIMENTAL METHODS

A. Base and Filler Materials

In the present study, the laser weldability of five different Al-Zn alloys was studied; these alloys mainly differed in their Zn, Mg, and Cu contents. For this purpose, the commercial alloys AA7075, AA7050, and AA7034 and the prealloys PA734 and PA765 were used

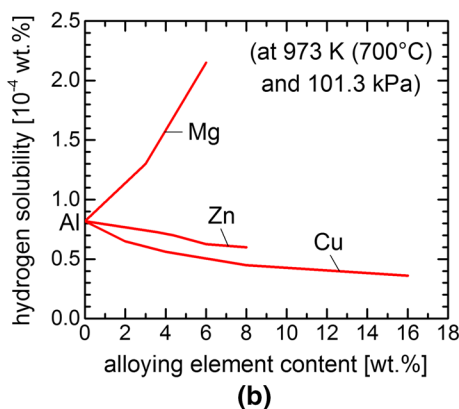
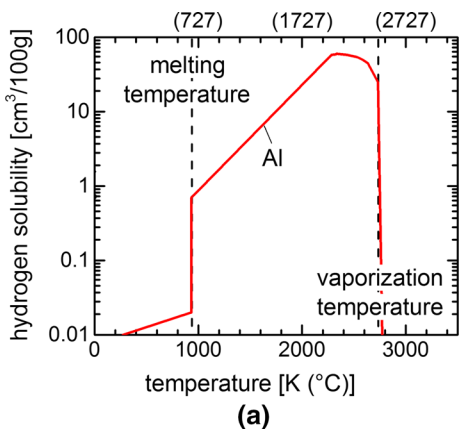


Fig. 7—(a) Hydrogen solubility of Al at different temperatures and (b) dependence of the hydrogen solubility on the alloying element content of different binary Al alloys (according to Verhaeghe^[6] and Anyalebechi^[23]).

Table II. Chemical Composition (Weight Percent) of the Used Al Alloys—Ordered by Increasing (Zn + Mg + Cu) Content

Alloy (Temper)	Si	Fe	Cu	Mn	Mg	Cr	Zn	Ti	Al
AA5087 (—)	0.24	0.4	0.05	1.1	5.2	0.25	0.25	0.15	bal
PA734 (T76)	0.03	0.04	2.13	0.01	1.64	—	6.77	0.02	bal
AA7075 (T6)	0.4	0.5	2.0	0.3	2.9	0.28	6.1	0.2	bal
AA7050 (T76)	0.12	0.15	2.6	0.1	2.6	0.04	6.7	0.06	bal
PA765 (T79)	0.05	0.1	0.61	0.14	2.72	0.15	9.47	0.02	bal
AA7034 (T6)	0.1	0.12	1.0	0.2	2.3	0.2	11.0	—	bal

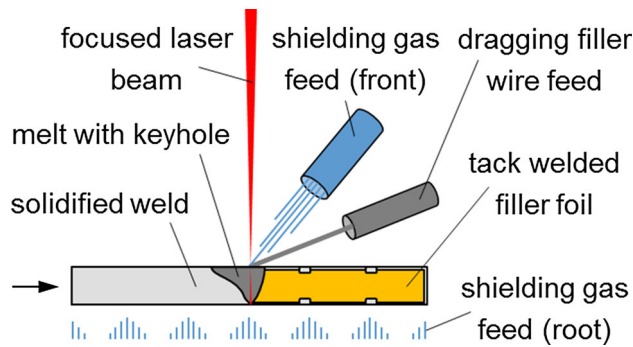


Fig. 8—Used configuration for the LBW of the butt joints.

as BMs. Alloys AA7034 and PA765 were only available as extruded profiles. In order to achieve comparable results, all sheets were conformed to a thickness of 2.0 mm either by milling or by spark erosion. Al-Mg alloys are generally recommended as filler material for the welding of Al-Zn alloys, in order to prevent crack formation within the weld seam. Therefore, AA5087 was chosen as filler wire with a diameter of 1.0 mm. When considering the approach for solving the weldability problems, a 99.8 pct pure V foil with a thickness of 40 μm was used in addition to the conventional filler wire. The chemical compositions of all used Al alloys and the corresponding temper conditions are specified in Table II.

B. Hydrogen Measurement

In order to assess the influence of hydrogen on laser weldability, the initial (surface and bulk) hydrogen contents of the Al-Zn alloys were measured using the hydrogen analyzer LECO* RH-402. The working prin-

*LECO is a trademark of LECO Corporation, St. Joseph, MI.

ciple of this device is hot gas extraction. Therefore, samples of the same size were extracted from the BMs. Providing similar surface conditions as used for welding, the sample preparation by grinding and cleaning with alcohol resembles the preparation for LBW. In this way, the falsification of the measurements and the deterioration of welds by oxide layers and surface contaminations were reduced to a minimum. The calibration of the

Table III. Used LBW Parameter Sets for Both Welding Scenarios

Parameter	Unit	Worst Case	Enhanced
Laser power	kW	2.0	2.0
Focal position	mm	0	0
Welding speed	mm/min	3500	3500
Feed rate of filler wire	mm/min	—	2500
Flow rate of shielding gas (front/root)	L/min	—	20/5

system was performed using gas dosing based on hydrogen, since solid standards with defined hydrogen content are not available.

C. Laser Beam Welding

The LBW of butt joints was performed using a three-axial computerized numerical control machining center, which was connected to a 2.2 kW Nd:YAG laser. The laser fiber had a diameter of 300 μm , and the laser optic had a focal length of 250 mm. This resulted in a focused beam diameter of approximately 366 μm . To retain the position of the sheets and to ensure a narrow gap during welding, a mechanical clamping device was used. The filler wire was supplied by a dragging wire feed. For accurate positioning of the V foil, a foil strip was laser tack welded on the face of one of the sheets. Argon was used as the shielding gas. It was supplied from the front and root side of the weld in order to provide complete shielding of the melt pool. The LBW configuration used is depicted in Figure 8.

Two different welding scenarios were carried out. At the beginning, the so-called “worst-case” welding scenario was performed. For this purpose, neither filler material (wire and foil) nor shielding gas was used. Thus, it was possible to investigate exclusively the influence of the chemical composition of the different Al-Zn alloys on their laser weldability. Furthermore, the limited feasibility of improving laser weldability by varying the LBW parameters as well as by the sole addition of conventional filler wire was demonstrated. Subsequently, the so-called “enhanced” welding scenario was performed in order to assess the effectiveness of the novel approach for improving laser weldability. The welding parameter sets of both scenarios are shown in Table III.

D. Nondestructive Testing

Visual inspection was used to assess the outer appearance of the weld seams with special attention paid to weld imperfections such as undercut, excess of penetration, and spikes, whereas radiographic inspection (according to DIN EN ISO 17636-1) was used to determine inner weld imperfections such as porosity and cracks. In addition, an image analysis of the radiographs was conducted in order to quantify the amount of pores and undercuts as well as the amount of excess of penetration and spikes. For this purpose, the tonal range of the scanned radiographs was adjusted with the help of image editing software. The chemical composition of the deposits observed on the welded specimens in the vicinity of the weld seam was determined by means of energy-dispersive X-ray spectroscopy (EDS). Therefore, the deposit was applied on a self-adhesive and conductive graphite foil.

E. Destructive Testing

The microstructural properties of the joints were investigated by optical microscopy. The local mechanical properties of the joints were determined by means of Vickers microhardness testing HV 0.2 (according to DIN EN ISO 6507-1). Therefore, several indentations were made at all regions of the joint—the fusion zone (FZ), heat-affected zone (HAZ), and BM.

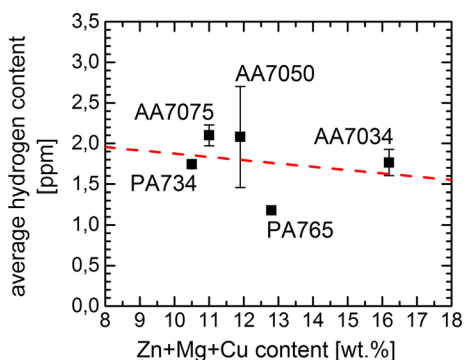


Fig. 9—Measured hydrogen content (with error bars) of the used Al-Zn alloys.

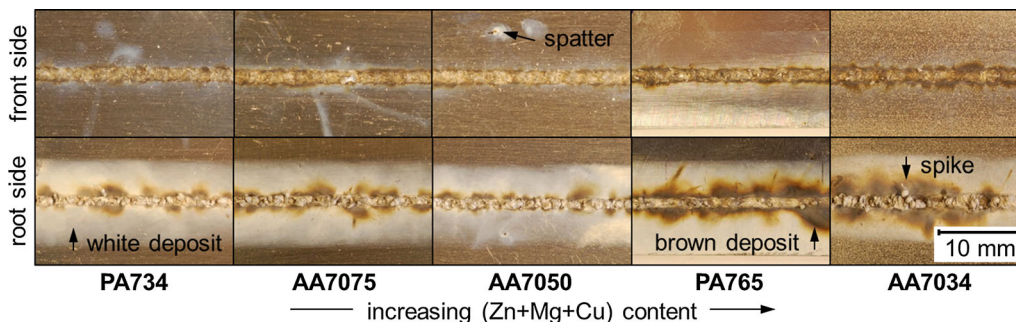


Fig. 10—Pictures of the front and root side of the worst-case welds.

V. RESULTS AND DISCUSSION

A. Hydrogen Measurements

The measured initial hydrogen content of the different Al-Zn alloys was approximately 1.2 to 2.1 ppm low. And, with an increasing amount of (Zn + Mg + Cu), the hydrogen content only slightly decreased, as can be seen in Figure 9. Although the Mg content has the largest influence on hydrogen solubility (also Figure 7(b)), the overall decrease of hydrogen content could be explained by the high Zn content (especially in comparison to the Mg and Cu contents), which was able to compensate for the effect of the Mg content. The larger deviation of the hydrogen content in AA7050 could be caused by discontinuities in the bulk material. Due to the low hydrogen content of all of the investigated alloys, hydrogen could be excluded as the main reason for the observed weldability problems.

B. Visual Inspection

The outer appearance of the worst-case welds is shown in Figure 10. It was generally characterized by the presence of undercut at the front side, weld sagging and drop-through (spikes) at the root side, as well as tiny spatter marks and deposits on the surface of the workpieces (especially at the root side). In addition, the visual inspection of the worst-case welds showed that with an increasing amount of (Zn + Mg + Cu), the laser weldability of Al-Zn alloys substantially deteriorated. Further, it became apparent that the proneness for sagging, spike formation, weld metal expulsion (spatter), and vaporization increased. The worst weld quality was observed for AA7034, which contained the highest amount of (Zn + Mg + Cu) among the investigated alloys.

The whitish and brownish deposits on the surface close to the welds originated from the vaporization of the volatile elements Mg and Zn during welding. The irregular disposition of the deposits along the weld line can be explained by the unsteadiness of the vaporization process and the collapsing of the keyhole during welding, as described previously. The reason for the increased tendency of sagging and spike formation lies in the low surface tension and viscosity of the melt, which was caused by high Zn and Mg contents (also Table I).

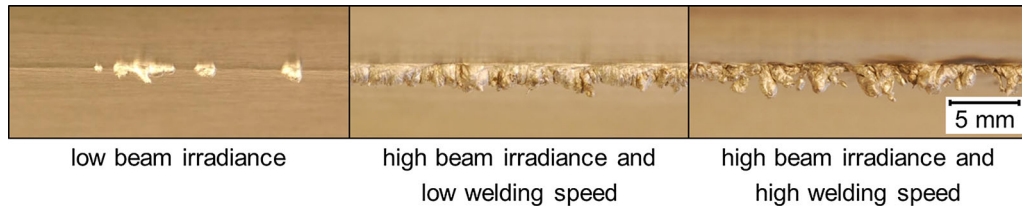


Fig. 11—Typical appearance of the root side for different welding parameters: (a) incomplete penetration, (b) weld sagging, and (c) and spike formation.

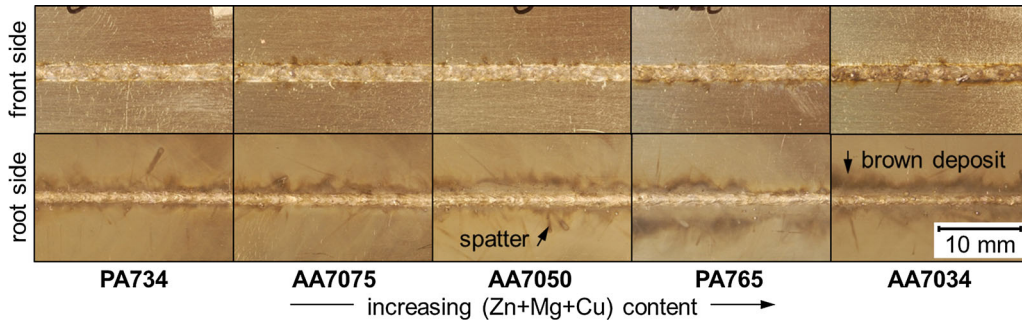


Fig. 12—Pictures of the front and root side of the enhanced welds.

Table IV. Measured Chemical Composition (Weight Percent) of the Deposits of Welded AA7075

Element	Worst Case	Enhanced
Al	16.82	14.72
Zn	54.59	60.95
Mg	27.46	23.26
Cu	0.70	0.65
V	—	0.33

The variation of LBW parameters as well as the sole addition of conventional filler wire led to no improvement of the weld seam appearance. Here, three different types of weld root could be identified, as shown in Figure 11. No or incomplete penetration occurred in the case of beam irradiances below the threshold irradiance. An increase of the beam irradiance, *e.g.*, by increasing the laser power, resulted either in sagging for low welding speeds or in the formation of spikes for high welding speeds. The latter case was accompanied by increased weld metal expulsion. By the feed of conventional Al-Mg filler wire during welding, the threshold irradiance was shifted to higher levels, because more material had to be molten. However, at the same time, the tendency for weld sagging also increased because of the low surface tension and viscosity of Mg containing Al alloys.

In contrast, the enhanced welds showed a uniform outer appearance of the weld seams for all Al-Zn alloys, as can be seen in Figure 12. Even in the case of AA7034, neither sagging nor spikes occurred at the weld root. At the surface of the root side of all welds, deposits could still be found. However, the color of the whitish deposit changed to light brown, due to the use of V, and the

distribution of the deposits along the weld line seemed to be reduced and more uniform.

The clear difference between the outer appearances of both welding scenarios was accounted for by the use of V as additional filler material, since the same laser power and welding speed were used for welding. The V has a considerably higher surface tension than Al, Mg, and Zn (Table I). The value for the viscosity of V was not available, but it is supposed to be high.^[15] This reduced the proneness to weld sagging and the formation of spikes during welding. Even the negative effect of the Al-Mg filler wire used—resulting in a further decrease of the surface tension—was compensated for by V. In addition, V exhibited a considerably lower vapor pressure than Al, Zn, and Mg (Figure 1(a)), which helped to stabilize the keyhole during LBW.

The obtained EDS results for the deposits of the worst-case and improved welds of AA7075 are shown in Table IV. The measured high content of Zn and Mg in the deposit confirmed the earlier assumptions of an increased vaporization of these volatile elements during LBW of Al-Zn alloys. In contrast, there were only traces of Cu and V—in the case of the enhanced weld—found in the deposit, due to their considerable higher vaporization temperature. The chemical composition of the deposits of both welds seemed to be similar, although an Al-Mg filler wire as well as a V foil was added for welding the enhanced weld. This indicated that the addition of V did not change the vaporization behavior during LBW but did change other thermophysical properties of the weld metal, which finally led to an improved laser weldability of Al-Zn alloys. The observed color difference of the deposit could be explained by the differing temperature conditions near the melt pool. Thus, the brownish deposit, which was always adjacent to the weld seam (Figures 10 and 12),

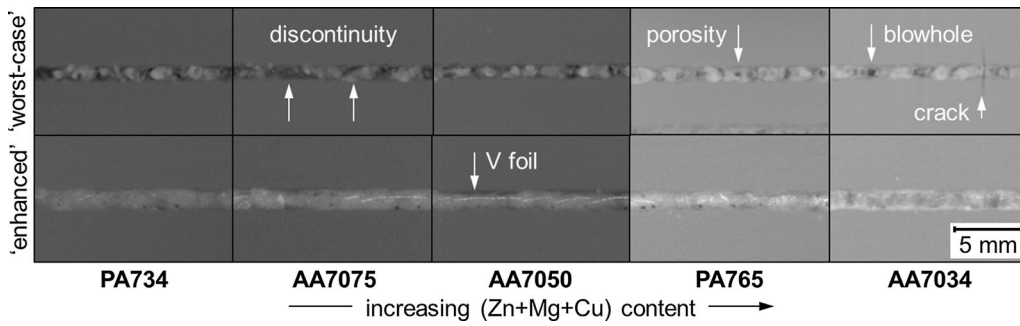


Fig. 13—Radiographs of the worst-case and enhanced welds.

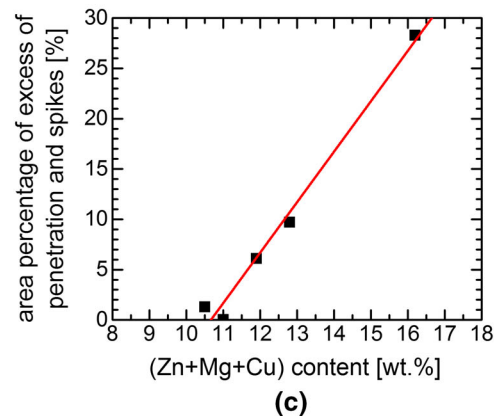
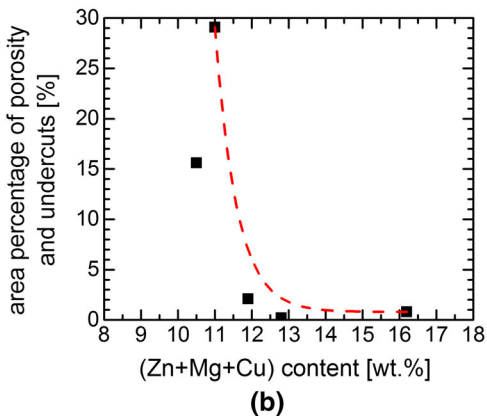
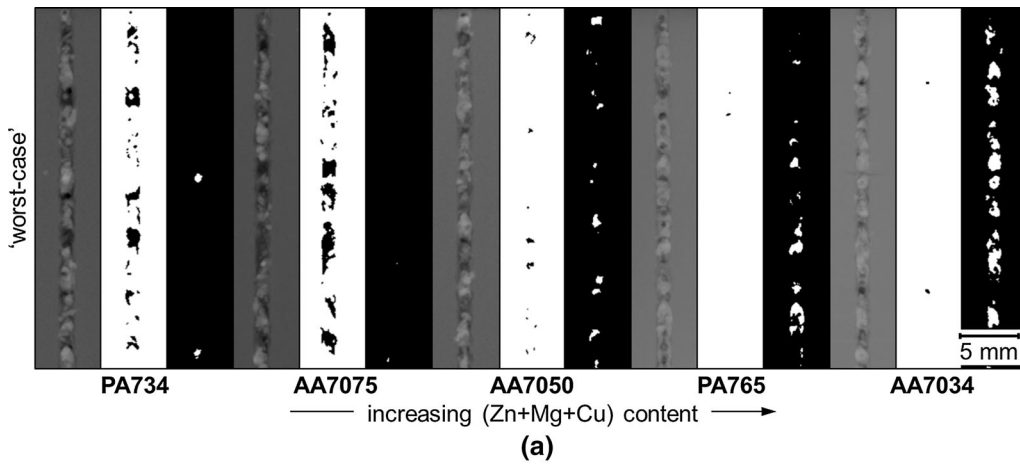


Fig. 14—Images (left: radiograph, middle: porosity and undercuts, and right: excess of penetration and spikes) used for analysis of (a) the radiographs and (b) the influence of the main alloying elements on the percentage of pores and undercuts and (c) on the excess of penetration and spikes of the worst-case welds.

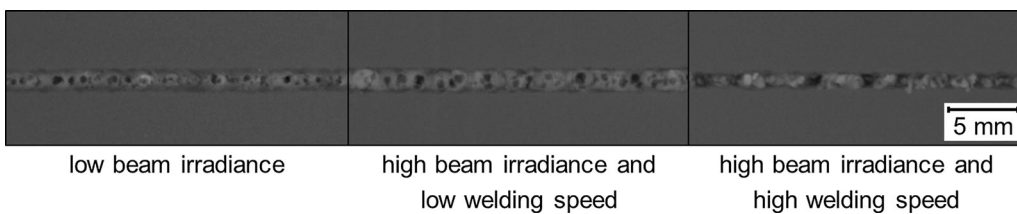


Fig. 15—Typical radiographs of weld seams welded with different parameters: (a) incomplete penetration, (b) weld sagging, and (c) spike formation.

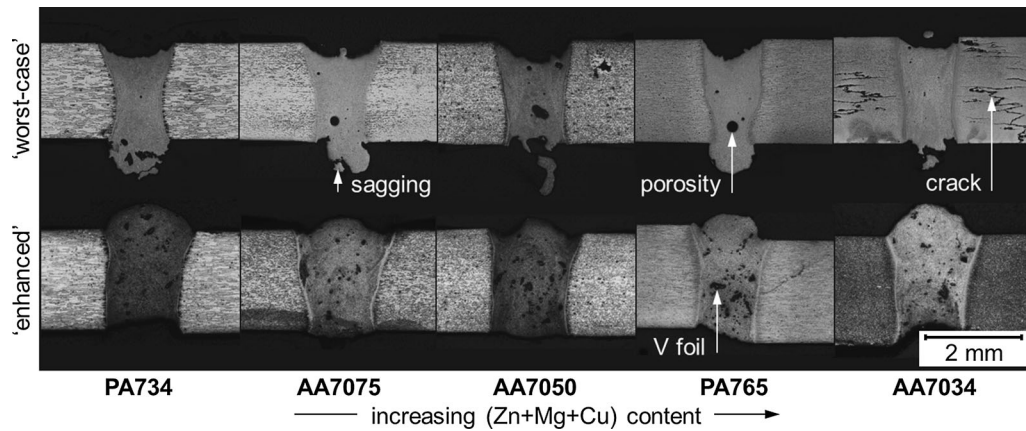
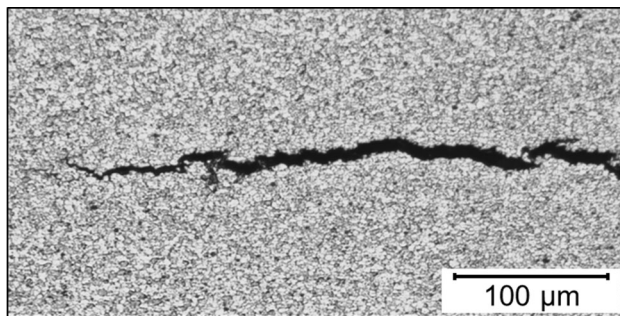
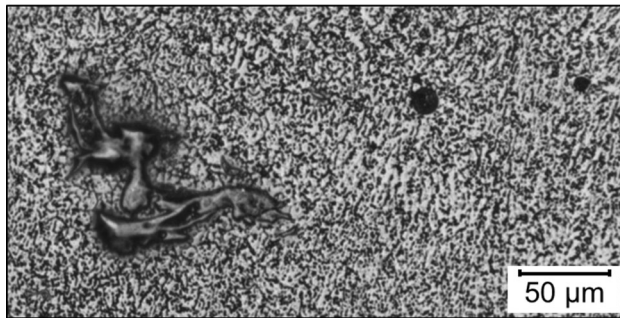


Fig. 16—Macrographs of the worst-case and enhanced welds.



(a)



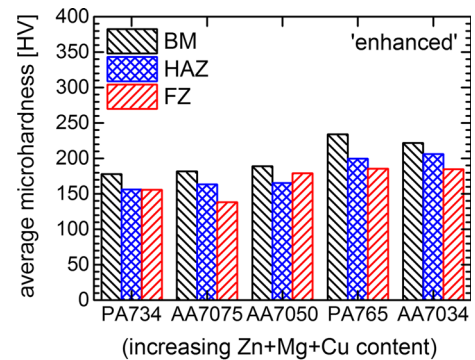
(b)

Fig. 17—(a) Hot crack in the HAZ of the AA7034 worst-case weld and (b) V-rich particle and residual porosity within the FZ of an enhanced weld.

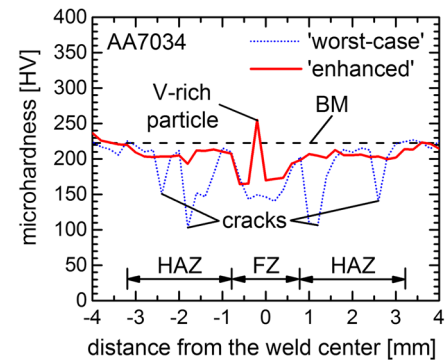
was caused by an overheating of the particles, whereas the whitish deposit resulted from the oxidation of the particles at elevated temperatures.

C. Radiographic Inspection

The radiographs of the worst-case and enhanced welds are shown in Figure 13. It can be seen that the worst-case welds of all Al-Zn alloys show only a limited number of pores, whereas severe weld irregularities occurred—appearing as density differences. In the worst-case weld of AA7034, macroscopic cracks were found, which run perpendicular to the welding direction,



(a)



(b)

Fig. 18—(a) Average microhardness at different positions of the enhanced weld and (b) comparison of the microhardness of a worst-case and an enhanced weld of AA7034.

as indicated with an arrow in Figure 13. In contrast, the radiographs of the enhanced weld seams consistently show only little porosity, and the weld seams appear to be denser and more uniform. Tiny remains of the unmelted or undissolved V foil could merely emerge.

The results of the image analysis of the radiographs of the worst-case welds are shown in Figure 14(a). It became obvious that with an increasing amount of (Zn + Mg + Cu), the amount of porosity and undercuts apparently decreased exponentially (Figure 14(b)), whereas the

amount of excess of penetration and spikes linearly increased (Figure 14(c)).

The exponential decay of porosity and undercuts from approximately 30 pct to low values in spite of the increasing amount of Zn and Mg—which are easy to vaporize—could be explained by the low surface tension of the high-alloyed Al-Zn alloys. On the one hand, it enabled the degassing of the melt pool; on the other hand, it also caused the expulsion of the melt and, thus, also of the pores. The linear increase of the amount of excess of penetration and spikes was also caused by the low surface tension, due to the alloying with Zn and Mg.

The residual porosity of all enhanced welds (Figure 13) detected in the radiographs was below 1 pct and was supposed to be hydrogen induced, due to the small size of the pores. The hydrogen might originate from the used Al-Mg wire, because this alloy exhibited the highest hydrogen solubility (Figure 7(b)). The increased density of the enhanced weld seams could be explained by the higher density of V and the absence of severe undercuts.

Clear porosity was solely observed for welds exhibiting either incomplete penetration or sagging, as can be seen in Figures 15(a) and (b). The reason for this was the unfavorable degassing condition during welding. In both cases, the keyhole was closed at the root side, due to the incomplete penetration of the sheet or to too high capillary pressure because of the large melt pool and the low surface tension (also Figure 2).

D. Metallography

The macrographs of the worst-case and enhanced welds are shown in Figure 16. In the worst-case welds, a considerable undercut at the front side, excess of penetration, and spikes at the root side of the welds were observed. Furthermore, the weld porosity was clearly visible. Only in the case of AA7034 were severe microcracks observed in the HAZ (Figure 17(a)). In contrast, the enhanced welds showed no undercut, sagging, or spikes. The observed pores had only small diameters. In all enhanced welds, V-rich particles were observed, which were almost homogeneously distributed within the weld seam. The typical size ratio between the residual porosity and the V-rich particles can be seen in Figure 17(b). AA7034 showed no cracks in the HAZ after the use of V as additional filler material.

The differences in size of the pores of both welding scenarios could be explained by the causes for porosity. The large and often noncircular pores are generally assigned for keyhole-induced porosity, whereas the small and circular pores are assigned for hydrogen-induced porosity, as described previously. The cracks in the HAZ of the worst-case weld of AA7034 were supposed to be liquidation cracks. Due to residual stresses in the welded specimen, these cracks could coalesce to a macroscopic crack, which was observed in the radiograph of this weld (also Figure 13). Liquidation cracks could not be avoided by the use of an appropriate filler wire because of their location in the HAZ. For the enhanced weld of this alloy, no more cracks were observed, due to the improved temperature distribution by the use of V foil.

E. Microhardness

The results of the microhardness measurements of the enhanced welds are shown in Figure 18(a). It can be seen that the hardness of the BM increased with the increasing amount of (Zn + Mg + Cu). A hardness drop within the HAZ was observed for all welds. The hardness levels of the FZ of the enhanced welds were either comparable to those of the HAZ or only slightly lower. A direct comparison of the results of a worst-case and an enhanced weld is shown in Figure 18(b).

The hardness peaks in the enhanced welds could be explained by the presence of a V-rich particle within the weld seam. The microhardness of pure V lay at about 628 HV. However, also, the shift of the microhardness level of the FZ could be explained by the strengthening effect by alloying V to an Al-Zn alloy. Due to the same parameters used for welding, which defined the heat input, the size and hardness drop within the HAZ were comparable. The hardness drop in the HAZ of the worst-case weld of AA7034 was caused by the microcracks in this region.

VI. CONCLUSIONS

On the basis of the knowledge obtained from this study, the following conclusions can be drawn.

1. The laser weldability of high-alloyed Al-Zn alloys deteriorates with an increasing total amount of Zn, Cu, and Mg. This can be explained by the thermophysical properties of the alloys, which were considerably influenced by the main alloying elements and their contents in the alloy. Even one unfavorable thermophysical parameter can have a detrimental effect on laser weldability.
2. Owing to the low initial hydrogen content of the BMs, hydrogen could be excluded as the main reason for the inferior laser weldability of high-alloyed Al-Zn alloys.
3. Since laser weldability of high-alloyed Al-Zn alloys strongly depends on the thermophysical properties of the alloy, it could hardly be improved by the variation of the welding parameters.
4. An improvement of laser weldability could merely be achieved by the use of the novel approach, which implies the use of V as additional filler material in order to positively affect the resulting thermophysical properties of the melt pool. The resulting weld seams showed a significantly improved outer appearance and a reduced amount of porosity.

REFERENCES

1. I.N. Fridlyander and O.G. Senatorova: *Mater. Sci. Forum*, 1996, vol. 217, pp. 1813–18.
2. K. Cudney: *Weld. Int.*, 1993, vol. 7 (8), pp. 599–603.
3. T. Ma: Ph.D. Thesis, Delft University of Technology, Delft, 1997.
4. W. Zhou: *Singapore Welding Society Newsletter*, Sept. 1999.

5. N Kamp, A Sullivan, and JD Robson: *Mater. Sci. Eng. A*, 2007, vol. 466, pp. 246–55.
6. G. Verhaeghe: Ph.D. Thesis, University of Warwick, Warwick, 2008.
7. S.C. Wu, X. Yu, R.Z. Zuo, W.H. Zhang, H.L. Xie, and J.Z. Jiang: *Weld. J.*, 2013, vol. 92 (3), pp. 64–71.
8. M. Olabode, P. Kah, and A. Salminen: *Rev. Adv. Mater. Sci.*, 2015, vol. 42, pp. 6–19.
9. M. Olabode: Ph.D. Thesis, University of Technology, Lappeenranta, Lappeenranta, 2015.
10. L. Zhang, X. Li, Z. Nie, H. Huang, and J. Sun: *Mater. Des.*, 2015, vol. 83, pp. 451–58.
11. S. Anik and L. Dorn: *Schweißtechnik Metallischer Werkstoffe*, DVS, Düsseldorf, 1995.
12. T. Ma and G. den Ouden: *Mater. Sci. Eng. A*, 1999, vol. 266 (1), pp. 198–204.
13. L.F. Mondolfo: *Aluminium Alloys: Structure and Properties*, Butterworth and Co., London, 1979, pp. 842–82.
14. J. Rapp, M. Beck, F. Dausinger, and H. Hügel: *Proc. 5th ECLAT, Bremen, Sept. 1994*, DVS-Verlag, Düsseldorf, 1994, pp. 313–25.
15. K.H. Leong and H.K. Geyer: *Proc. ICALEO, Orlando, FL, Nov. 1998*, Laser Institute of America, Orlando, FL, 1998, vol. 85 (2), pp. F-243–F-251.
16. K.H. Leong, H.K. Geyer, K.R. Sabo, and P.G. Sanders: *Proc. ICALEO, San Diego, CA, Nov. 1997*, Laser Institute of America, Orlando, FL, 1997, vol. 83 (2), pp. G-1–8.
17. A. Block-Bolten and T.W. Eager: *Metall. Trans. B.*, 1984, vol. 15B, pp. 461–69.
18. H. Zhao and T. DebRoy: *Weld. J.*, 2001, vol. 80, pp. 204–10.
19. WM Haynes: *CRC Handbook of Chemistry and Physics*, 92th ed., CRC Press, Boca Raton, 2011, pp. 6-88–6-117.
20. E. Beyer: *Schweißen mit Laser—Grundlagen*, Springer, Berlin, 1995, pp. 28–40.
21. W.M. Steen, J. Dowden, M. Davis, and P. Kapadia: *J. Phys. D Appl. Phys.*, 1988, vol. 21, pp. 1255–60.
22. G. Guizzetti and A. Piaggi: *Handbook of Optical Constants of Solids 2*, 1st ed., Academic Press, New York, 1998, pp. 477–85.
23. P.N. Anyalebechi: *Scripta Metall.*, 1995, vol. 33, pp. 1209–16.
24. M. Mazur: *Weld. Int.*, 1992, vol. 6, pp. 929–31.
25. S. Riekehr, H. Iwan, R. Dinse, V. Ventzke, and P. Haack: European Patent No. EP20120162865, 2012.
26. J. Enz, S. Riekehr, V. Ventzke, and N. Kashaev: *Mater. Sci. Forum*, 2015, vols. 828–829, pp. 389–94.